RSC Advances

ROYAL SOCIETY OF CHEMISTRY

www.rsc.org/advances

Graphical Abstract

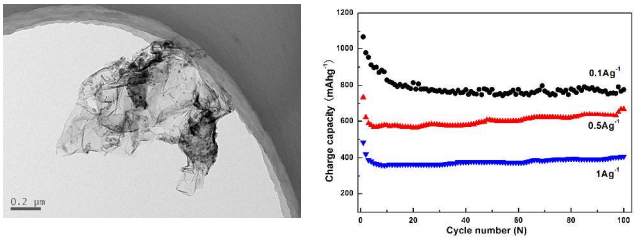

Cite this: DOI: 10.1039/c0xx00000x

www.rsc.org/xxxxxx

ARTICLE TYPE

Carbon nanospheres grown on graphene as anodes for Li-ion batteries

Youlan Zou, Xiangyang Zhou[1], Juan Yang[2]

A graphene/carbon nanospheres electrode for Li-ion batteries is synthesized via in-situ polymerization and carbonization. Carbon nanospheres derived from carbonized polypyrrole are grown on the surface of graphene and assembled into a flake-like structure. The synergistic effect between carbon and graphene improves the capacity and rate capability of the electrode.

The most commonly used graphitic or graphitization carbon reluctantly meets the ever-increasing and urgent demand for its limited capacity of 372 mAh g^{-1}.[1,2] To increase the capacity of the Li-ion batteries, alternative anode materials with higher capacities are needed. Polypyrrole (PPy) is an attractive material for the high conductivity and high value of specific capacity[3]. While rapid expansion and shrinkage of the polymer occur during charge/discharge process, which would destroy the integrity of the structure and lead to quick fading of capacity. In order to overcome this drawback, PPy is modified and composited with buffering materials[4,5]. In this paper, flake-like graphene/carbon nanospheres has been fabricated as an anode for Li-ion batteries. This material exhibits excellent charge capacity, high cyclic capability and rate performance.

Graphite oxide was first synthesized by a modified Hummers' method[6]. 120 mg graphite oxide was dispersed into 100 mL pure water by ultrasonication for 2 h to get an exfoliated yellow-brown GO suspension. Then, the suspension was heated at 160 ℃ for 2 h in a sealed autoclave. The resultant graphene solution was obtained for further using. $FeCl_3 \cdot 6H_2O$ (9.8 g) and sodium phenylsulfonate (SDBS, 3 g) were dissolved in the above-mentioned graphene solution under ice bath. Then, pyrrole monomer (1 mL) was added. After being magnetically stirred for at 0 ℃ for 5 h. A black precipitate of graphene/PPy nanospheres was generated, washed and dried under vacuum at 0 ℃ for 2 days, followed by heating in a tube furnace under high-purity Ar at 805 ℃ for 2 h at a heating rate of 3 ℃·min^{-1}. For comparison, the carbon nanospheres without graphene added was prepared under the same condition.

Scanning electron microscopy (SEM, JSM-6360LV, Japan), atomic force microscopy (AFM, NanoScope (R) III) and transmission electron microscopy (TEM, JEM-2100F, Japan) images were taken to characterize the morphologies and structures of the samples. Laser raman spectroscopy (OLYMPUS, BX41) with an excitation wave length of 488 nm by a KAr matrix was used to observe the type of carbonized materials. The electrode was prepared by mixing 80% sample, 10% carbon black, and 10% polyvinylidene fluoride (PVDF) and dissolving into N-methylpyrrolidinone (NMP) to form slurry, which was then coated onto a copper foil and dried overnight at 120℃ in a vacuum for 12h. The coin cell was assembled in a glove box filled with pure argon (Super 1220/750). Metallic lithium was used as the negative electrode and counter electrode. The electrolyte was 1molL^{-1} $LiPF_6$ dissolved in a mixture of ethylene carbonate/diethyl carbonate (1:1, by volume). Galvanostatic discharge/charge experiments were performed over a potential range of 3 V～0.01 V vs. Li^+/Li using a LAND testing (CT-2001A). Electrochemical workstation (Solartron 1470E) was taken to measure the cyclic voltammograms (CV) at a scanning rate 0.2 mVs^{-1}. Here the total weight of the graphene/carbon composite was considered to calculate the capacity values.

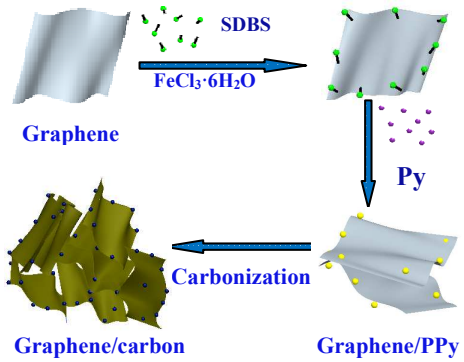

Scheme 1. Schematic illustration of the three-step formation process of graphene/carbon composite

The formation mechanism of graphene/carbon composite is schematically depicted in scheme 1. The approach is designed on the basis of the unique amphiphilic character of graphene with negatively charged hydrophilia and hydrophobic property[7]. When the negative charged ammonium ion of SDBS is combined with graphene dispersions, the surfactant micelles will adsorb on the surface of the graphene sheets. $FeCl_3 \cdot 6H_2O$ acts as the oxidant. Then, Py monomer is added and induced on the surface of the graphene sheets by SDBS. In-situ chemical oxidation polymerization occurs just on the surface of graphene to form graphene/PPy composite. Finally, the graphene/PPy composite is placed into the tube furnace to transfer the PPy into carbon and further remove the functional groups of graphene.

Fig. 1 depicts the morphologies and structures of the pure carbon powder and the graphene/carbon composite. The SEM

[1] School of Metallurgy and Environment, Central South University, Changsha, China, 410083, Tel/Fax:+86 073188836329
E-mail address: lanlinliao@163.com;
[2] E-mail address: zylan0935@csu.edu.cn;

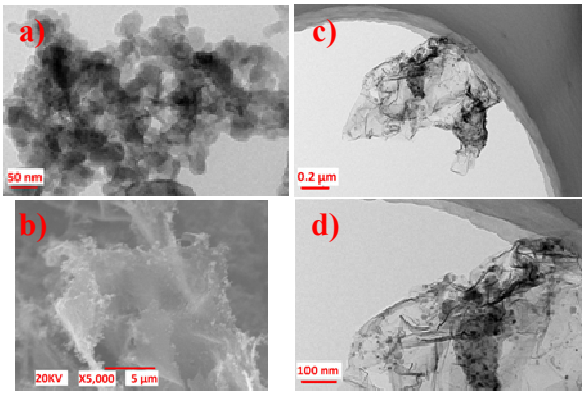

Fig. 1 a) SEM image of carbon powder, b) SEM, c) and d)TEM images of graphene/carbon composite

image (Fig.1a) of the carbon powder shows a homogeneous morphology of single nanospheres with about 20 nm in diameter. The SEM image of the graphene/carbon composite (Fig. 1b) shows the flake-like morphology with several micrometers (typically 12-15μm) in size. TEM images (Fig. 1c, d) demonstrate that the graphene/carbon composite remains the spherical structure of the pure carbon powder. The spherical carbon are distributed on the flexible and crumpled graphene nanosheets.

AFM image (Fig. 2) confirms that the average particle size of the carbon nanospheres for graphene/carbon composite is in the range of 6～8 nm, which is much smaller than that of pure carbon powder (seen from Fig.1a). It is probably that graphene facilitates the dispersion of Py monomer and hinder the growth of PPy granules.

XRD patterns in Fig. 3a are presented to reveal the composition and crystallinity of graphene and graphene/carbon. The graphene nanosheets show only a weak (002) diffraction line at $2\theta=24^{o8}$. Compared with graphene, another two peaks at around 20°～25° can be observed for graphene/carbon composite, indicating the amorphous phases are introduced to the obtained composite. Raman spectra proves to be an essential tool to characterize graphene and other carbon materials. The D-band is a measure of disorder originating from defects and the G-band is representative of sp^2-hybridized carbon bonds[9]. Raman spectrum of graphene/carbon composite (Fig. 3b) displays a strong G-band at 1580.4 cm^{-1} and a weak D-band at 1366.4 cm^{-1}. The G/D intensity ratio (0.97) is a little lower than that of G (1.01). This is due to the anti-synergistic effect that the ordered

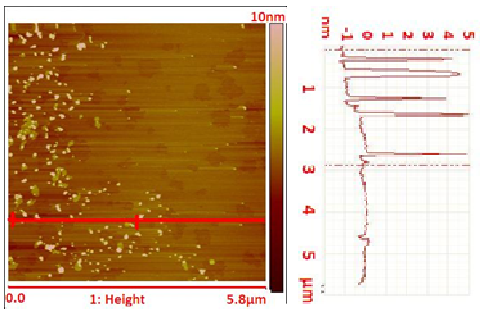

Fig. 2 AFM image of graphene/carbon composite

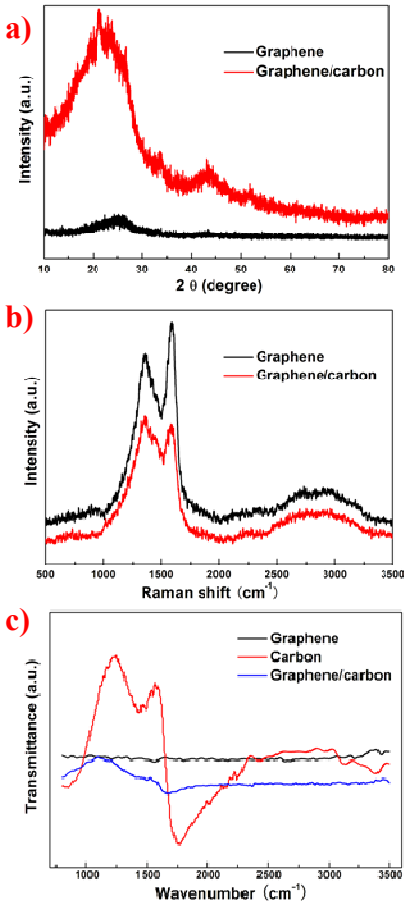

Fig. 3 a) XRD, b) Raman c) FTIR spectra of graphene/carbon

graphene and disordered carbon nanospheres are both introduced to graphene/carbon composite[10]. The D+G/2D intensity ratio is used to demonstrate the defect concentration of graphene[11]. Another two peaks for graphene/carbon composite located at about 2692.3 cm^{-1} and 2930.5 cm^{-1} can be ascribed to the 2D and D+G modes, respectively. The D+G/2D intensity ratio for graphene/carbon composite decreases in comparison with that of pure graphene, suggesting that the defect concentration for graphene/carbon composite is much reduced. FTIR spectra of the pure graphene, pure carbon powder and graphene/carbon composite are shown in Fig. 3c. The FTIR spectrum of graphene illustrates that the band of O-H at around 1320 cm^{-1},O-H at 3490 cm^{-1}, and C=O at 1760 cm^{-1} gradually disappear, clarifying the peaks for oxygen functional groups gradually removed and formed reduced graphene sheets. It is clearly seen from FTIR spectrum of the pure carbon powder that the peak at 3390 cm^{-1} is due to N–H stretching of the PPy ring. The peaks at 3030 and 2910 cm^{-1} are designated as the asymmetric stretching and symmetric vibrations of methylene. The band at 1770 cm^{-1} corresponds to the C=C backbone stretching. The bands at 1250 and 1570 cm^{-1} may be assigned to the stretching vibration of the doping state and vibrations C–N stretching of PPy, respectively. After the carbon powder was composited with graphene, the spectrum of graphene/carbon presents the structure changes of both the graphene and carbon powder.

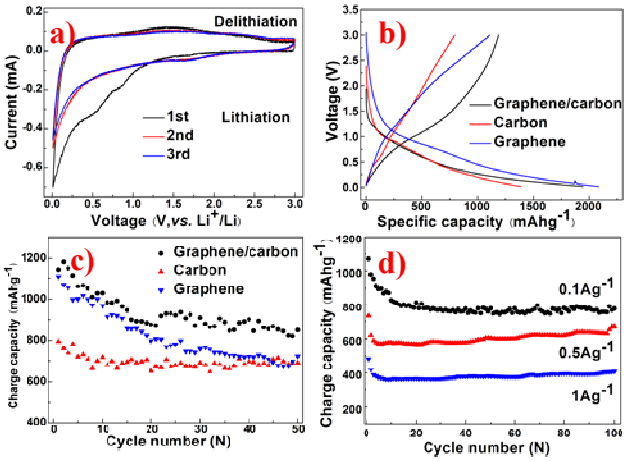

Figure 4. a) CV curves, b) the first charge-discharge curves, c) cyclic performance and d) rate capability of graphene/carbon

Electrochemical performance of the graphene/carbon composite is investigated in coin cells using lithium as the counter electrode. Fig. 4a illustrates the CV curves of the graphene/carbon composite. From the first cycle, the irreversible peaks at 0.8 and 0.5 V are associated with the electrolyte interphase (SEI) films at the electrode-electrolyte interface and the irreversible Li-ions insertion into an inclosed spaces that are confined by crumpled graphene, respectively[12]. No irreversible peak is observed in the 2nd and 3rd cycles, indicating the integrated SEI films have been formed in the 1st cycle. The reversible peaks at about 0.01 and 0.2 V are related to the reversible Li-ions reaction with graphene and carbon nanospheres, respectively[13]. In the first cycle (Fig. 4b), graphene/carbon electrode delivers a very high reversible charge capacity of 1187.7 $mAhg^{-1}$ at 0.05 Ag^{-1} in the voltage range of 0.01 to 3.0 V (vs Li^+/Li), which is almost three times higher than the theoretical capacity of graphite (372 $mAhg^{-1}$) and is also higher than that of pure carbon powder(793.6 mAh/g). For comparison, the initial charge capacity for graphene is investigated to be 1108 $mAhg^{-1}$ at 0.05 Ag^{-1}, indicating graphene provide extra capacity for graphene/carbon. It is interesting to be noted that the charge capacity of graphene/carbon is higher than the pure carbon powder and pure graphene, which indicates that the existence of carbon powder and graphene provide other lithium storage mechanisms on the electrode apart from the classical graphite intercalation compound mechanism. The introduce of graphene to form flake-like structures limits the volume expansion of carbon nanospheres. The surface of graphene leads to sufficient electrode/electrolyte interface to absorb Li-ions and promotes rapid charge-transfer reaction. Graphene also supplies a large number of active sites for Li-ion migration, enhances the conductivity and shortens the electronic transport route. Moreover, carbon nanospheres inserted between graphene layers expand the gap of the interlayers which in turn allow easier migration of Li-ions. The carbonization of PPy would a good approach to introduce N heteroatom into carbon materials, which is beneficial for improving the capacity of the electrode[14]. In addition, the spaces enclosed by carbon nanospheres and graphene are beneficial for ion/electron transfer and the sufficient contact between active materials and electrolyte. After the first 20 cycles, the electrode becomes highly reversible. More importantly, the graphene/carbon composite exhibits a stable cycling performance the same with pure carbon powder (Fig. 4c). The capacity of graphene/carbon remains 850 $mAhg^{-1}$ after 50 cycles at 0.05 Ag^{-1}, compared with that of 690 $mAhg^{-1}$ for pure carbon nanospheres, and 721.9 $mAhg^{-1}$ for pure graphene. The results demonstrate that the synergistic effect between carbon nanospheres and graphene sheets improves the cycling stability of the graphene/carbon electrode. Rate capability is another important factor for the use of graphene/carbon electrode in Li-ion batteries. It is required to provide its high specific capacities at high current density. The rate performance of graphene/carbon is presented in Fig. 4d. The capacity of graphene/carbon decreases gradually with the increase of the current density from 0.1 to 1 Ag^{-1}. While the specific capacity increases gradually during cycling at each current, indicating the stable structure and the sufficient permeation of the electrolyte into the interior of the electrode. When the current densities increase to 0.1, 0.5 and 1 Ag^{-1}, the anodes maintain the charge capacities of 776.4, 670.9 and 407.2 $mAhg^{-1}$ after 100 cycles respectively. The results imply that the flake –like graphene/carbon electrode is very effective for improving the rateperformance.

In this study, a simple approach was developed to prepare flake-like graphene/carbon nanospheres. PPy nanospheres grown on the graphene layers were transformed into carbon nanospheres after carbonization. The carbon nanospheres with an average diameter of 6～8 nm are homogeneously distributed between the graphene sheets as spacers to separate the neighboring graphene. Graphene serves as a highly conductive support material and provides the large surface for the well-dispersed deposition of carbon nanospheres. The flake-like structure are beneficial for fast ion/electron transfer and sufficient contact between active materials and electrolyte. This material exhibits an improved capacity, rate capability and cycling stability.

This work is financially supported by Nature Science Foundation of China. (NO: 51204209,51274240).

1. H.Y. Wang, Y. Masaki Y. *J. Power Sources*, 2001, **91**, 123.
2. Y. Masaki, H. Y. Wang, F. Kenji, U. Tatsuo, A. Takeshi, O. Zempachi. *J. Mater. Chem.*, 2004, **14**, 1754.
3. W. Sun, X. Y. Chen. *J. Power Sources*, 2009, **193**, 924.
4. L. Qie, W. M. Chen, Z. H. Wang, Q. G. Shao, X. Li, L. X. Yuan, X. L. Hu, W. X. Zhang, Y. H. Huang. *Adv. Mater.*, 2012, **24**, 2047.
5. H. L. Wang, Y. Yang, Y. Y. Liang, J. T. Robinson, Y. G. Li, A. Jackson, Y. Cui, H. J. Dai. *Nano Lett.*, 2011, **11**, 2644.
6. L. Noerochim, J. Z. Wang, S. L. Chou, D. Wexler, H. K. Liu. *Carbon*, 2012, **50**, 1289.
7. L. L. Zhang, S. Y. Zhao, X. N. Tian, X. S. Zhao. *Langmuir*, 2010, **26**, 17624.
8. S. Q. Chen, Y. Wang, H. Ahn, G. X. Wang. *J. Power Sources*, 2012, **216**, 22.
9. Z. J. Fan, W. Kai, J Yan, T. Wei, L. J. Zhi, J. Feng, Y. M. Ren, L. P. Song, F. Wei. *ACS Nano*, 2011, **5**, 191
10. L. M. Malard, M. A. Pimenta, G. Dresselhaus, M. S. Dresselhaus. *Phys Rep.*, 2009, **473**, 51.
11. H. L. Wang, J. T. Robinson, X. L. Li, H. J. Dai. *J. AM. CHEM. SOC.*, 2009, **131**, 9910.
12. V. Basker, P. Jason, H. Bala, P. Branko. *J. Power Sources*, 2002, **109**, 377.
13. W. Guoxiu, X. P. Shen, J. Yao, J. Park. *Carbon*, 2009, **47**, 2049.
14. L. G. Bulusheva, A. V. Okotrub, A. G. Kurenya, H. K. Zhang, H. J. Zhang, X. H. Chen, H. H. Song. *Carbon*, 2011, **49**, 4013.